Chapter Six

An Ansatz for Easy-Plane Antiferromagnet Kinks

6.1 Introduction: Other π-Kink Systems

We want to formulate an Ansatz for kinks in the easy-plane antiferromagnet with an applied field in the easy plane, similar to that for the Liebmann et al. Ansatz. A major difference from that case will be imposed by the boundary conditions here, which make the kink describable by two trajectories on the unit sphere which trace out angles approximately equal to π, rather than 2π as for the ferromagnet. There will be one trajectory for each sublattice. Furthermore, the spin-flopped ground state complicates the algebra compared to what would necessary if the two sublattices were exactly antiparallel.

In order to show that this Ansatz is well-motivated and expected to give good results, we first look at some other π-kink Hamiltonians, where this Ansatz gives the exact known soliton solutions. These "practice" example have exactly antiparallel boundary conditions at $z \to \pm\infty$, which simplifies the geometry, and therefore the calculations.

The first example will be the easy-plane ferromagnet with no applied magnetic field, which is known to have pulse-like π solitons (Mikeska 1981). The second example is the same ferromagnet, but with the addition of an Ising symmetry-breaking field in the easy plane, described by a term $-C \sum_n (S_n^y)^2$ in the Hamiltonian. This term makes the positive and negative y-axis directions the prefered directions within the easy plane, and a π kink involves a trajectory on the unit sphere from one to the other.

6.2 Ansatz for the Easy-Plane Ferromagnet, No Applied Field

In units and coordinates used in Chapter 2, the continuum Hamiltonian and equations of motion for the easy-plane ferromagnet in the absence of a field are

$$H = \varepsilon_0 \int d\xi\{\tfrac{1}{2}\theta_\xi^2 + \tfrac{1}{2}\phi_\xi^2 \cos^2\theta + \tfrac{1}{2}\sin^2\theta\} \tag{6-1}$$

$$\dot{\theta} = \phi_{\xi\xi}\cos\theta - 2\phi_\xi\theta_\xi\sin\theta \tag{6-2a}$$

$$\dot{\phi}\cos\theta = -\theta_{\xi\xi\xi} + (1 - \phi_\xi^2)\sin\theta\cos\theta \quad . \tag{6-2b}$$

The right hand side of (6-2a) is an exact differential, and this allows one to find the following pulse soliton solution (Mikeska 1981).

$$\sin\theta = \pm\gamma^{-1}\,\mathrm{sech}\,\gamma^{-1}(\xi - u\tau) \tag{6-3a}$$

$$\phi = \phi_0 \mp \tan^{-1}[\tfrac{1}{u}\sin\gamma^{-1}(\xi - u\tau) \tag{6-3b}$$

$$\gamma \equiv (1 - u^2)^{-1/2} \quad . \tag{6-3c}$$

Here ϕ_0 is an arbitrary integration constant and u is the dimensionless soliton velocity. For the upper signs, and $\phi_0 = 0$, it is instructive to note that xyz components of unit spin vectors $\hat{\sigma}$ are

$$\sigma^x = u\,\mathrm{sech}\,\gamma^{-1}(\xi - u\tau) \tag{6-4a}$$

$$\sigma^y = -\tanh\gamma^{-1}(\xi - u\tau) \tag{6-4b}$$

$$\sigma^z = \gamma^{-1}\,\mathrm{sech}\,\gamma^{-1}(\xi - u\tau) \tag{6-4c}$$

By rotating to an x'y'z' coordinate system through an angle θ_A about the y-axis, such that $\sin\theta_A = \gamma^{-1}$, $\cos\theta_A = u$, this is seen to be a sine-Gordon profile in the x'y' coordinates

$$\sigma^{x'} = \sigma^{x} \cos\theta_A + \sigma^{z} \sin\theta_A = \text{sech}\, \gamma^{-1}(\xi - u\tau) \tag{6-5a}$$

$$\sigma^{y'} = -\sigma^{y} \qquad = -\tanh \gamma^{-1}(\xi - u\tau) \tag{6-5b}$$

$$\sigma^{z'} = -\sigma^{x} \sin\theta_A + \sigma^{z} \cos\theta_A = 0 \quad . \tag{6-5c}$$

It is easy to verify that the angle $\phi' \equiv \tan^{-1}(\sigma^{y'}/\sigma^{x'})$ is given by

$$\phi' = \tfrac{1}{2}\pi - 2 \tan^{-1} \exp \gamma^{-1}(\xi - u\tau) \quad , \tag{6-6}$$

which is the π sine-Gordon profile, as seen in chapter 5. Therefore, the exact pulse soliton is described by a trajectory which is the intersection of the unit sphere with a plane tilted at an angle θ_A from the easy plane, about an axis in the easy plane through the origin (the choice of the y-axis was arbitrary and related to using $\phi_0 = 0$). The distribution of the spins on the trajectory is a sG distribution. The velocity of the pulse is directly related to the tilt angle θ_A via $u = \cos\theta_A$. Also, the width is related to the angle by $w = 1/\sin\theta_A$. Finally, the energy is

$$\varepsilon_{\text{pulse}} = 2\varepsilon_0(1 - u^2)^{1/2} \quad . \tag{6-7}$$

This result is strange in that the soliton energy is a decreasing function of velocity. A pulse soliton which is tilted at only a small angle to the xy plane has high velocity but low energy. The opposite is true for one tilted at $\theta_A \sim 90°$.

Now the Ansatz calculation is sketched out. A sine-Gordon distribution in a tilted plane is assumed, similar to equations (6-5) and (6-6), with a variational width parameter w and variational angle of tilt θ_A. The Ansatz for unit spins $\hat{\sigma}$ is written

$$\sigma^{x'} = \sin\phi_{sG} = \text{sech}[(\xi - u\tau)/w] \tag{6-8a}$$

$$\sigma^{y'} = \cos\phi_{sG} = -\tanh[(\xi - u\tau)/w] \tag{6-8b}$$

$$\sigma^{z'} = 0 \tag{6-8c}$$

where

$$\phi_{sG} = 2\ \tan^{-1}\exp[(\xi - u\tau)/w] \quad . \tag{6-9}$$

The spins here rotate clockwise from the +y'-axis to the -y'axis as viewed down the z'-axis, when going from $\xi = -\infty$ to $\xi = +\infty$. This is transformed back to the original xyz coordinates by a rotation through angle θ_A about the y'-axis:

$$\sigma^{x} = \sigma^{x'}\ \cos\theta_A - \sigma^{z'}\ \sin\theta_Z = \cos\theta_A\ \mathrm{sech}[(\xi - u\tau)/w] \tag{6-10a}$$

$$\sigma^{y} = \sigma^{y'} \qquad\qquad = -\tanh[(\xi - u\tau)/w] \tag{6-10b}$$

$$\sigma^{z} = \sigma^{x'}\sin\theta_A + \sigma^{z'}\cos\theta_A \quad = \sin\theta_A\ \mathrm{sech}[(\xi - u\tau)/w] \quad . \tag{6-10c}$$

This is the Ansatz. One must extremize the Lagrangian L for the system, with respect to the variational parameters w and θ_A. In terms of xyz spin components, the Lagrangian is

$$L = K - H \tag{6-11a}$$

$$K = \varepsilon_0 \int d\xi\ \sigma^z \frac{d}{d\tau} \tan^{-1}(\sigma^y/\sigma^x) \tag{6-11b}$$

$$H = \varepsilon_0 \int d\xi\ \{\tfrac{1}{2}\left(\frac{\partial\hat{\sigma}}{\partial\xi}\right)^2 + \tfrac{1}{2}(\sigma^z)^2\} \quad . \tag{6-11c}$$

The functional K can be shown to be the product of the soliton momentum P and the velocity u. After some easy integration, the simple results are

$$K = 2u\theta_A\ \varepsilon_0 \tag{6-12a}$$

$$H = (w \sin^2\theta_A + 1/w)\varepsilon_0 \quad . \tag{6-12b}$$

Then, extremizing L first with respect to w, and the θ_A, leads to the results

$$w = (\sin\theta_A)^{-1} = (1 - u^2)^{-1/2} \tag{6-13a}$$

$$E = 2 \sin\theta_A \, \varepsilon_0 = 2(1 - u^2)^{1/2}\varepsilon_0 \tag{6-13b}$$

$$u = \cos\theta_A \tag{6-13c}$$

$$P = 2\theta_A \quad . \tag{6-13d}$$

The known pulse soliton solution has been recovered, as should be expected since the Ansatz carries the exact functional form necessary. All dynamical quantities are obtained directly in terms of the variation parameter θ_A, which in effect has beome the independent variable, replacing the velocity.

6.3 Ansatz for the Easy-Plane Ferromagnet with Ising Symmetry Breaking

One can also apply Ansatz (6-10) to the situation where there is an Ising symmetry breaking field. Then the Hamiltonian is

$$H = \varepsilon_0 \int d\xi \, \{\tfrac{1}{2}(\frac{\partial\hat{\sigma}}{\partial\xi})^2 + \tfrac{1}{2}(\sigma^z)^2 - c(\sigma^y)^2\} \tag{6-14}$$

In this case, we obtain

$$K = 2u\theta_A\varepsilon_0 \tag{6-15a}$$

$$H = [w(\sin^2\theta_A + 2c) + 1/w]\varepsilon_0 \tag{6-15b}$$

and

$$w = (\sin^2\theta_A + 2c)^{-1/2} \tag{6-16a}$$

$$E = 2(\sin^2\theta_A + 2c)^{1/2}\varepsilon_0 \tag{6-16b}$$

$$u = \sin\theta_A \cos\theta_A(\sin^2\theta_A + 2c)^{-1/2} \tag{6-16c}$$

$$P = 2\theta_A \quad . \tag{6-16d}$$

Once again, the profile that results is the exact soliton solution (Sklyanin 1979).

6.4 Ansatz for the Easy-Plane Antiferromagnet with Applied Field

With the above examples, and based on some numerical simulations, it is possible to formulate the Ansatz for the spin-flopped ground state antiferromagnet. Conceptually, this is a minor modification of the above Ansatz. We want the spins on the A sublattice to move in a plane tilted at an angle θ_A away from the easy (xy) plane, and the spins on the B sublattice to move in a plane tilted at some angle θ_B from the easy plane. Sine-Gordon profiles within these planes are assumed, with a width parameter w. Thus, the Ansatz will involve the three variational parameters θ_A, θ_B and w, which will be determined by extremizing the Langrangian with respect to these parameters.

The spin-flopped ground state (section 5.2) makes the Ansatz (6-10) inapplicable to this case, since it does not satisfy the boundary conditions. Also, the spins on a sublattice in general do not trace out a trajectory through exactly π radians. For example, in a static xy kink, the A sublattice would trace out an angle $\pi - 2\phi_0$, while the B sublattice would trace out $\pi + 2\phi_0$, where $\cos\phi_0 = \frac{1}{4}\beta$ (section 5.3). But for a moving kink, both angles would be changed, and depend on θ_A and θ_B.

An Ansatz is constructed for unit spins $\hat{\sigma}_A$ on the A sublattice first. What is needed for the trajectory is the intersection of the unit sphere with a plane which passes through the two ground state (boundary condition) points $(\frac{1}{4}\beta, \pm(1-\beta^2/16)^{1/2}, 0)$, tilted at angle θ_A to the easy (xy) plane. The trajectory for the A sublattice will begin at one ground state $(\frac{1}{4}\beta,-(1-\beta^2/16),^{1/2}\ 0)$, pass through a point (cos q, 0, sin q) at the center of the kink (where σ^z will be maximum) and then end at the opposite ground state $(\frac{1}{4}\beta, +(1-\beta^2/16)^{1/2}, 0)$. The tilt angle of this plane, θ_A, is related to the parameter q by (see Figure 6.1)

$$\tan \theta_A = \sin q/(\cos q - \tfrac{1}{4}\beta) \quad . \tag{6-17}$$

The angle q is the out-of-plane angle θ (the maximum) for the spin at the center of the kink (on the A sublattice here). In the x'y'z' system, obtained by rotating from the xyz system through θ_A about the y-axis, the equation of this plane is simply

$$z' = -\tfrac{1}{4}\beta \sin\theta_A \quad . \tag{6-18}$$

So determining the z' component of $\hat{\sigma}_A$ was trivial.

Next, to obtain the x' and y' components of this trajectory, consider the sum and difference vectors $\vec{M}$ and $\vec{N}$, defined by

$$\vec{M} = \tfrac{1}{2}(\hat{\sigma}_A + \hat{\sigma}_B) \tag{6-19a}$$

$$\vec{N} = \tfrac{1}{2}(\hat{\sigma}_A - \hat{\sigma}_B) \quad , \tag{6-19b}$$

where the $\hat{\sigma}_B$ sublattice is supposed for the moment to move in the same plane as $\hat{\sigma}_A$. Equation (6-19) applies only to the x'y' components. The $\hat{\sigma}_B$ sublattice stays approximately antiparallel to $\hat{\sigma}_A$, except at the boundary points at $z = \pm\infty$. From the boundary conditions specified by the ground

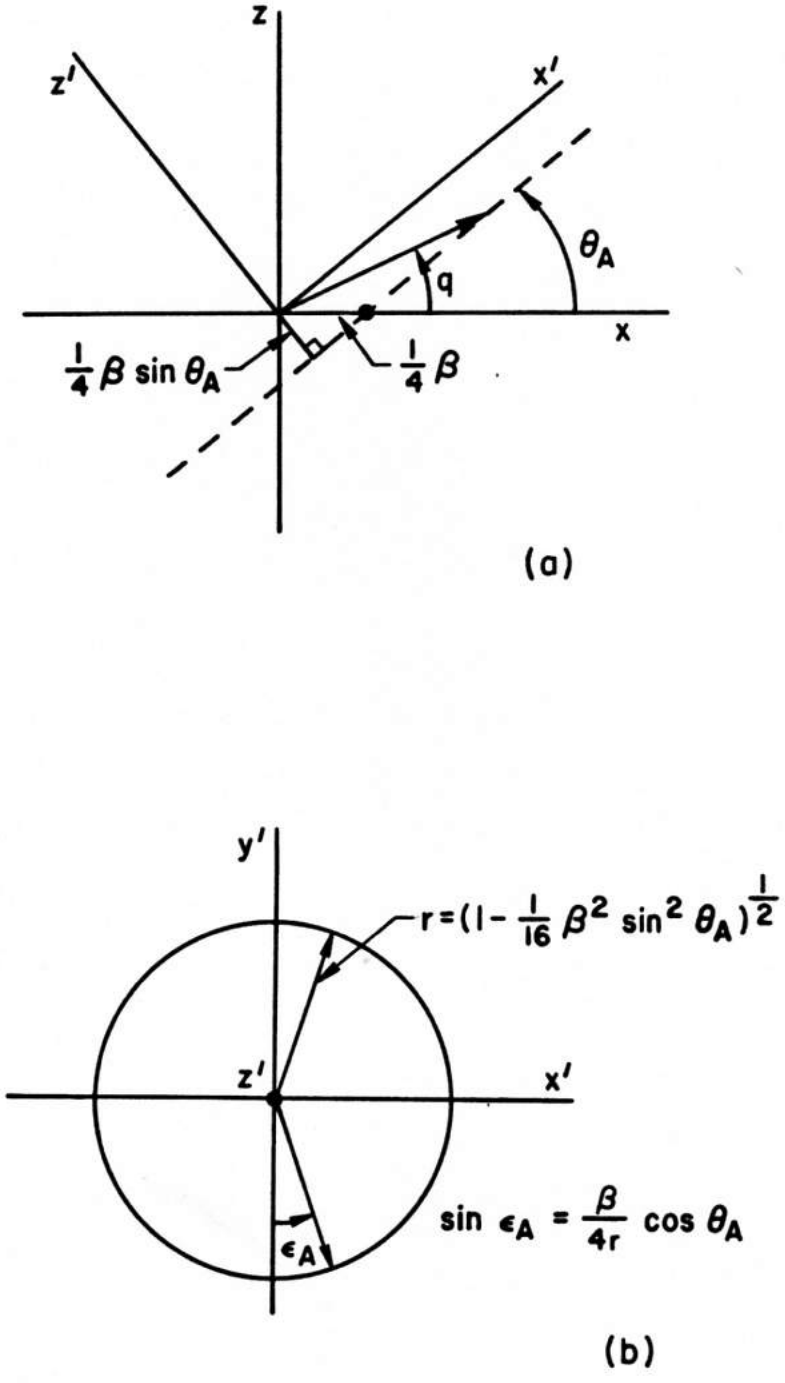

Figure 6.1 Geometry for the antiferromagnet kink Ansatz. (a) The dot represents the ground states projected onto the x-axis. The arrow is the spin on the A sublattice at the center of the kink. The dashed line represents the plane in which the tips of the spin vectors $\hat{\sigma}_A$ move in this Ansatz. (b) View of the two ground states as seen looking down the z-axis. The Ansatz assumes that the spins $\hat{\sigma}$ move in the circular path connecting them.

state, the vector $\vec{M}$ approximately traces out a circle of radius $r'_M = \frac{1}{8}\beta\cos\theta_A$, with center at $(x'y') = (\frac{1}{8}\beta\cos\theta_A, 0)$. Similarly, the vector $\vec{N}$ approximately traces out a semicircle of radius $r_N = (1 - \beta^2/16)^{1/2}$, centered at $(x',y') = (0,0)$. This is shown in Figure 6.2. From the geometry, the x'y' components of $\vec{M}$ and $\vec{N}$ are approximately

$$M_{x'} \simeq r'_M(\ 1 + \cos\phi_{sG}) = 2r'_M \tanh^2 x \qquad (6\text{-}20a)$$

$$M_{y'} \simeq r'_m \sin\phi_{sG} = -2r'_m \tanh x \operatorname{sech} x \qquad (6\text{-}20b)$$

$$N_{x'} \simeq r_N \sin \tfrac{1}{2}\phi_{sG} = r_N \operatorname{sech} x \qquad (6\text{-}20c)$$

$$N_{y'} \simeq -r_N \cos \tfrac{1}{2}\phi_{sG} = r_N \tanh x \quad , \qquad (6\text{-}20d)$$

where it has been <u>assumed</u> the ϕ_{sG} is

$$\phi_{sG} = 4 \tan^{-1} \exp x \quad , \qquad (6\text{-}21a)$$

$$x = (z - vt)/w \quad . \qquad (6\text{-}21b)$$

Here the length unit is the lattice spacing and the time unit is (/JS). The variable w is the width parameter. We check the squared lengths of the $\hat{\sigma}_A$ and $\hat{\sigma}_B$ spins as seen in the x'y' plane; they should equal r^2, where

$$r^2 = 1 - (\sigma^{z'})^2 = 1 - \frac{\beta^2}{16}\sin^2\theta_A \quad .$$

One obtains here

$$(\vec{M} \pm \vec{N})^2 = M^2 + N^2 = r_N^2 + 4r_M'^2 \tanh^2 x \quad . \qquad (6\text{-}22)$$

Since this has position dependence, it cannot equal r^2. In order to force the $\hat{\sigma}_A$ spins to be unit vectors, we need to multiply $\vec{M}$ and $\vec{N}$ by a factor $f_A(x) = r(r_N^2 + 4r_M'^2\tanh^2 x)^{-1/2}$. $f_A(x)$ can be written in terms of the angle ε_A (Figure 6.1)

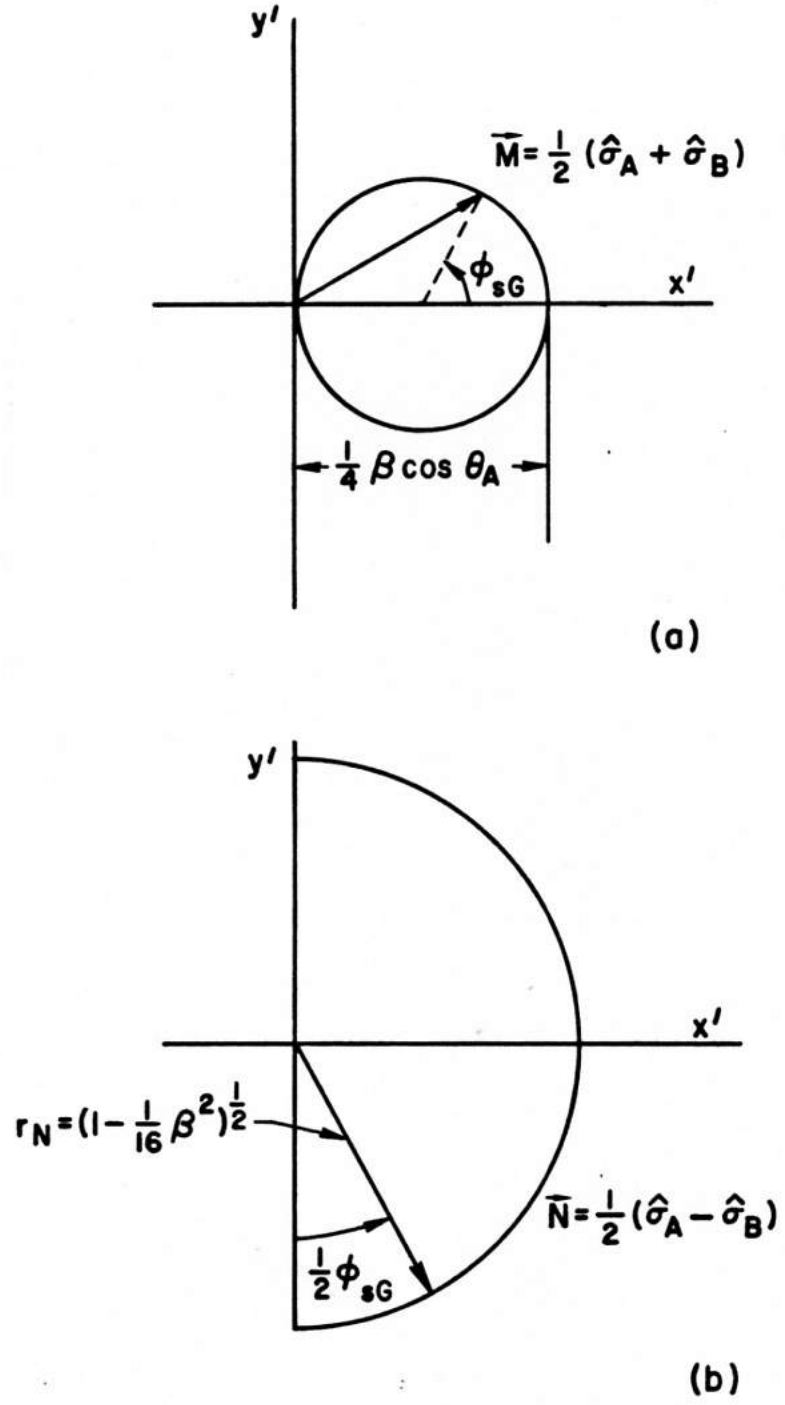

Figure 6.2 (a) The sum vector $\vec{M}$ as seen in the x'y' coordinate system. ϕ_{sG} rotates through 2π for the kink Ansatz. (b) The difference vector $\vec{N}$ as seen in the x'y' system. The radii of these circles are derived from Figure 6.1.

$$f_A(x) = \left(1 - \frac{\beta^2 \cos^2\theta_A}{16r^2} \operatorname{sech}^2 x\right)^{-1/2}$$

$$= (1 - \sin^2\varepsilon_A \operatorname{sech}^2 x)^{-1/2} \quad , \tag{6-23a}$$

where

$$\sin\varepsilon_A = \frac{\beta}{4r} \cos\theta_A \quad . \tag{6-23b}$$

With this, the Ansatz for the x'y'z' components for the $\hat{\sigma}_A$ spins is

$$\sigma_{Ax'} = f_A(x)(M_{x'} + N_{x'}) \tag{6-24a}$$

$$\sigma_{Ay'} = f_A(x)(M_{y'} + N_{y'}) \tag{6-24b}$$

$$\sigma_{Az'} = -\tfrac{1}{4}\beta \sin\theta_A \quad . \tag{6-24c}$$

Now the assumption that the B sublattice moves in the same plane is removed; $\hat{\sigma}_B$ has its own plane at an angle θ_B. Using double primes to refer to a coordinate systems at an angle θ_B to the easy plane, the B sublattice tilted plane is $z' = -\frac{1}{4}\beta\sin\theta_B$. The Ansatz for x"y"z" components of the $\hat{\sigma}_B$ spins is then

$$\sigma_{Bx''} = f_B(x)(M_{x''} - N_{x''}) \tag{6-25a}$$

$$\sigma_{By''} = f_B(x)(M_{y''} - N_{y''}) \tag{6-25b}$$

$$\sigma_{Bz''} = -\tfrac{1}{4}\beta\sin\theta_B \quad . \tag{6-25c}$$

$M_{x''}$ and $M_{y''}$ are different from the corresponding single prime quantities by having $r''_M = \frac{1}{8}\beta\cos\theta_B$. The distribution of the spins on the trajectories for both sublattices is described by the single function ϕ_{sG}. These Ansätze for the sublattices are rotated back to the original xyz coordinates by the transformation in equation (6-10).

One must now extremize the Lagrangian in order to determine the variational parameters θ_A, θ_B and w. Measuring energy in units of JS^2, time in units of /JS, the continuum limit Lagrangian is

$$L = K - H \tag{6-26a}$$

$$K = \frac{1}{2} \sum_{i=A,B} \int dz\, \sigma_{iz} \frac{d}{dt} \tan^{-1} (\sigma_{iy}/\sigma_{ix}) \tag{6-26b}$$

$$H = \int dz\{\hat{\sigma}_A \cdot \hat{\sigma}_B - \frac{1}{2} \frac{\partial \hat{\sigma}_A}{\partial z} \cdot \frac{\partial \hat{\sigma}_B}{\partial z} + \frac{1}{2}\alpha(\sigma_{Az}^2 + \sigma_{Bz}^2) - \frac{1}{2}\beta(\sigma_{Ax} + \sigma_{Bx})\} \quad . \tag{6-26c}$$

Note that subscripts here indicate spin components, not derivatives. $\alpha = 2A/J$ and $\beta = g\mu_B B_x/JS$, as before. Evaluating H for this Ansatz is straightforward but tedious. The "kinetic" term K, however, requires more work. It can be simplified somewhat by changing $\sigma_{AZ} \to \sigma_{AZ} - 1$, and $\sigma_{BZ} \to \sigma_{BZ} + 1$, which changes K by an additive constant depending only on β, and at the same time removes unphysical step functions[1] at $\theta_A = \frac{1}{2}\pi$ and $\theta_B = -\frac{1}{2}\pi$. This constant shift is irrelevant since L is extremized with respect to θ_A, θ_B and w. Details of these calculations are given in Appendix B.

$L(\theta_A,\theta_B,w)$ can be evaluated for arbitrary θ_A and θ_B, however, it is expected that $\Delta \equiv \theta_B - \theta_A \ll 1$, based on the sG limits in Chapter 5. Therefore, L is approximated to second order in Δ. Furthermore, the coefficients of the powers of Δ are also approximated to second order in the small parameters $\sqrt{\alpha}$ and β. Then finally the Lagrangian relative to the ground state can be written

---

[1] This is reminiscent of the step function in the Liebmann et al. Ansatz at $\theta_m = \frac{1}{2}\pi$. Perhaps there <u>is</u> some significance to these step functions?!

$$L(\theta_A, \Delta, w) = vP - \frac{1}{w}F - wG \tag{6-27}$$

where

$$P(\theta_A,\Delta) = \Delta + \frac{1}{4}\pi\beta(\sin\theta_A + \frac{1}{2}\Delta\cos\theta_A) \equiv p_0 + p_1\Delta \tag{6-28a}$$

$$F(\theta_A,\Delta) = (r_N^2 - \frac{\beta^2}{48}\cos^2\theta_A) - (\frac{\pi\beta}{16} r_N\sin\theta_A)\Delta - \frac{1}{6}\Delta^2 \equiv f_0 + f_1\Delta + \frac{1}{2}f_2\Delta^2 \tag{6-28b}$$

$$G(\theta_A,\Delta) = (\alpha r_N^2\sin^2\theta_A + \frac{1}{4}\beta^2\cos^2\theta_A) + \frac{1}{2}\sin2\theta_A(\alpha r_N^2 - \frac{1}{4}\beta^2)\Delta + \Delta^2 \equiv g_0+g_1\Delta + \frac{1}{2}g_2\Delta^2. \tag{6-28c}$$

Extremizing L first with respect to the width w leads to

$$w(\theta_A,\Delta) = (F/G)^{1/2} \tag{6-29a}$$

$$L(\theta_A,\Delta) = vP - E \tag{6-29b}$$

$$E(\theta_A,\Delta) = 2(FG)^{1/2} \simeq e_0 + e_1\Delta + \frac{1}{2} e_2\Delta^2 \quad . \tag{6-29c}$$

The energy E has been expanded to quadratic order in Δ, where the coefficients are

$$e_0(\theta_A) = 2(f_0g_0)^{1/2} \tag{6-30a}$$

$$e_1(\theta_A) = \frac{1}{2}(f_1/f_0 + g_1/g_0)e_0 \tag{6-30b}$$

$$e_2(\theta_A) = [\frac{1}{2}(f_2/f_0 + g_2/g_0) - \frac{1}{4}(f_1/f_0 - g_1/g_0)^2]e_0 \quad . \tag{6-30c}$$

These are functions of θ_A only, with α and β as parameters.

Next, extremize with respect to Δ, to obtain

$$\Delta(\theta_A) = (vp_1 - e_1)/e_2 \tag{6-31a}$$

$$L(\theta_A) = L_0 + L_1v + L_2v^2 \quad , \tag{6-31b}$$

where

$$L_0(\theta_A) = \tfrac{1}{2}e_1^2/e_2 - e_0 \qquad (6\text{-}32a)$$

$$L_1(\theta_A) = p_0 - p_1e_1/e_2 \qquad (6\text{-}32b)$$

$$L_2(\theta_A) = \tfrac{1}{2}p_1^2/e_2 \quad . \qquad (6\text{-}32c)$$

Now L is a function of θ_A only. Finally, variation with respect to θ_A leads to the quadratic equation for v:

$$L_0' + L_1'v + L_2'v^2 = 0 \quad . \qquad (6\text{-}33)$$

Primes denote differentiation with respect to θ_A. The two solutions $v_+(\theta_A)$ and $v_-(\theta_A)$ are

$$v_\pm(\theta_A) = (-L_1' \pm \sqrt{L_1'^2 - 4L_0'L_2'})/2L_2' \quad . \qquad (6\text{-}34)$$

These solutions for v can be accepted only if they give $\Delta \ll 1$, as we assumed. The variational parameter θ_A now becomes the independent variable. For a given θ_A, v_+ or v_- is found, and then used in equation (6-31a) to get Δ. The Δ so obtained is then used in combination with θ_A to get the width w, the momentum P and energy E. Thus all dynamical quantities are determined as function of θ_A only, with α and β as parameters. Unfortunately, the derivatives in equation (6-33) are rather complicated, and it is easiest to compute them numerically. Also, to find the kink dispersion E(v), it is easiest to eliminate θ_A numerically. Results will be shown below. But first, it is informative to consider two special two-parameter limiting forms of the Ansatz, one for xy kinks and one for yz kinks. These are shown to reproduce the sine-Gordon xy and yz limits.

6.5 yx Kink Limit of the Ansatz: $\theta_A = \theta_B$

A zero velocity xy sG kink obviously has $\theta_A = \theta_B$. Thus one might expect to a first approximation to reproduce some xy kink properties by re-formulating the Ansatz with this assumption, $\theta_A = \theta_B$, or $\Delta = 0$. This should work best for small velcoty, $v/c \ll 1$. Then, with this restriction, the functions P, F and G which determined L reduce to (equations 6-28))

$$P(\theta_A) = \frac{\pi}{4}\beta s \tag{6-35a}$$

$$F(\theta_A) = r_N^2 - \frac{\beta^2}{48}(1 - s^2) \tag{6-35b}$$

$$G(\theta_A) = \frac{1}{4}\beta^2 + (\alpha_N^2 - \frac{1}{4}\beta^2)s^2 \tag{6-35c}$$

$$s \equiv \sin\theta_A \quad . \tag{6-35d}$$

To get the dispersion relation E(v), L is extremized with respect to $\sin\theta_A$, obtaining E(s) and v(s), from which s can be elimated for small velocity. The width and energy are still given by equation (6-29). The velocity is given by

$$v(s) = \frac{\partial E/\partial s}{\partial P/\partial s} \quad . \tag{6-36}$$

It is straightforward to show

$$v(s) = \frac{4}{\pi\beta}(1 - \beta^2/12)^{1/2}(4\alpha - \beta^2)(s/\beta) \quad . \tag{6-37a}$$

$$E_{xy}(s) = \beta(1 - \beta^2/12)^{1/2}[1 + \frac{1}{2}(4\alpha - \beta^2)(s/\beta)^2] \quad . \tag{6-37b}$$

Terms higher order than s^2 have been dropped; these equations are applicable only for $s \ll 1$. Also these are to leading order in $\sqrt{\alpha}$ and β. For the static kink, $s = 0$, and the energy is $E^o_{xy} = \beta(1 - \beta^2/12)^{1/2}$, slightly

smaller than that obtained using spherical coordinates in the sG limit, equation (5-29). For kinks moving at small velocity, the sine of the tilt angle θ_A is proportional to the velocity. The constant of proportionality changes sign at the critical field $\beta_c^2 = 4\alpha$. Similarly, the curvature of E_{xy} changes sign at the critical field. Eliminating s leads to the dispersion relation.

$$E_{xy}(v) \simeq E^{o}_{xy} + \frac{1}{2}m^{*}v^2 \tag{6-38}$$

correct to order v^2, where m* is an effective mass:

$$m^{*} = \frac{(\pi\beta/4)^2}{(1-\beta^2/12)(4\alpha-\beta^2)}\, E^{o}_{xy} \quad . \tag{6-39}$$

At fields below the critical field, the mass m* is positive, however, m* diverges and changes sign as β is increased past the critical field. This strange result has already been found by Flüggen and Mikeska (1983), obtained essentially by solving equation (5-25b) via another Ansatz. Similarly, the width has the following behavior:

$$w(s) = \frac{2}{\beta}(1 - \beta^2/12)^{1/2}[1 - \frac{1}{2}(4\alpha - \beta^2)(s/\beta)^2] \quad . \tag{6-40}$$

w has the opposite curvature from E. Above the critical field the kink width increases with velocity while the energy decreases with velocity. At the critical field, both the width and energy are independent of velocity for $v \ll c$. This is probably indicative of a kink instability similar to that seen in the ferromagnetic kinks. Certainly this behavior is strongly perturbed from the sine-Gordon theory. Next we do a similar reduced Ansatz calculation for the yz limit, also to compare with the sine-Gordon theory.

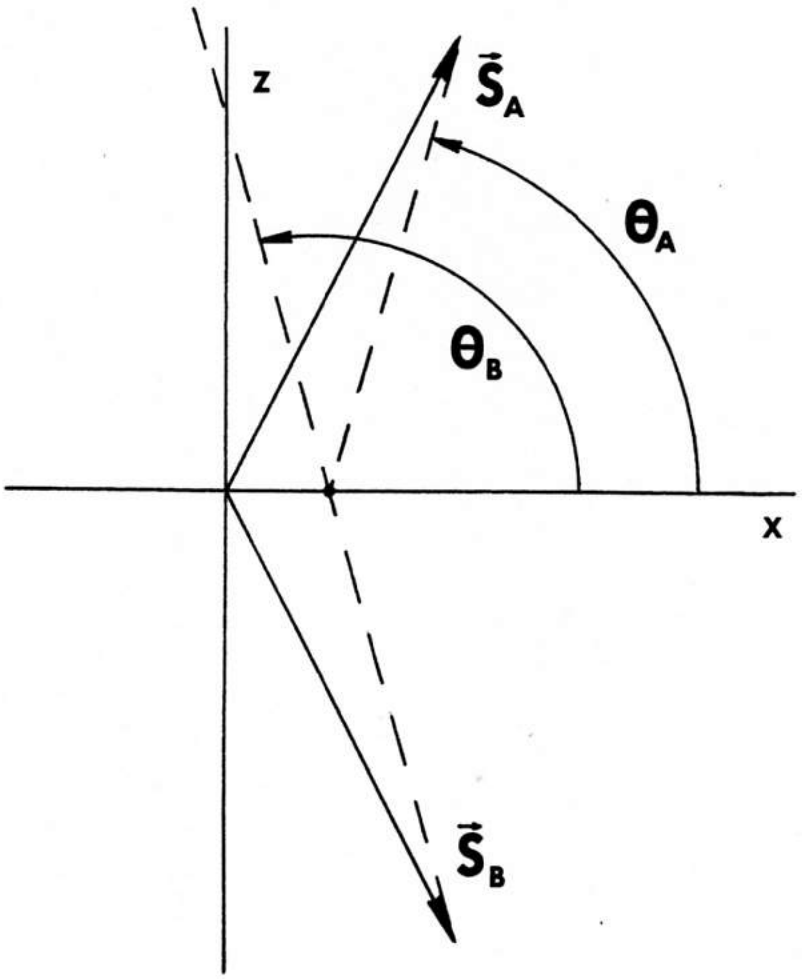

Figure 6.3 Geometry for the yz kink limit of the general three parameter Ansatz. $\vec{S}_A$ and $\vec{S}_B$ here are the spins at the center of the kink on the two sublattices. The dashed lines represent the two sublattice planes in which the tips of the spin vectors move. θ_A and θ_B are displaced in opposite directions from $\frac{1}{2}\pi$.

6.6 yz Kink Limit of the Ansatz: $\theta_A + \theta_B = \pi$

For a static yz kink, the two sublattice planes are both nearly parallel to the yz plane, such that $\theta_A \simeq \theta_B \simeq \frac{1}{2}\pi$. For a moving yz kink, we have seen that the two sublattices either are canted toward to away from the field. Therefore, we can make a yz kink Ansatz by assuming $\theta_A = \frac{1}{2}\pi - \varepsilon$ and $\theta_B = \frac{1}{2}\pi + \varepsilon$ (see Figure 6.3). Now ε becomes the variational parameter. Using the expressions given in Appendix B for the arbitrary θ_A, θ_B Ansatz, the functions P, F and G become

$$P(\varepsilon) = 2\pi + 2\varepsilon + \frac{1}{4}\pi\beta \cos\varepsilon \tag{6-41a}$$

$$F(\varepsilon) = r_N^2 - \frac{1}{8}\pi\beta r_N \cdot s - (\frac{2}{3} - \frac{7\beta^2}{48})s^2 \tag{6-41b}$$

$$G(\varepsilon) = \alpha r_N^2 - \frac{1}{8}\pi\beta\alpha r_N \cdot s + (4r_N^2 - \alpha)s^2 \tag{6-41c}$$

now

$$s \equiv \sin\varepsilon \quad . \tag{6-41d}$$

Again, higher order terms in s have been dropped in F and G, as well as higher order terms in $\sqrt{\alpha}$ and β. These expressions are valid for $\varepsilon \ll 1$. As was done for the xy limit, one finds the velocity and energy to be

$$v(s) = 2\sqrt{\alpha}\, r_N^2[-\frac{\pi\beta}{16 r_N} + (\frac{2}{\alpha} - \frac{5}{6r_N^2})s] \tag{6-42a}$$

$$E_{yz}(s) = 2\sqrt{\alpha}\, r_N^2[1 - \frac{\pi\beta}{8 r_N}\, s + (\frac{2}{\alpha} - \frac{5}{6r_N^2})s^2] \quad . \tag{6-24b}$$

Immediately it appears that this result is in error, since s = 0 does not correspond to v = 0, as supposed. In fact, for a zero velocity kink, a very small ε is required, given by

$$\varepsilon(v = 0) = (\frac{\pi\beta}{16r_N})/(\frac{2}{\alpha} - \frac{5}{6r_N^2}) \quad . \tag{6-43}$$

Conversely, for $\varepsilon = 0$, the kink has a small velocity

$$v(\varepsilon = 0) \equiv v_0 = -\frac{1}{8}\pi\beta r_N \alpha^{1/2} \ll 1 \quad . \tag{6-44}$$

This reflects the fact that the minimum energy configuration for small ε has the sublattices canted toward the field rather than being in the same plane. By doing so, the anisotropy and field energies are reduced while the exchange increases only slightly, so the net result is a reduction of the energy. Note that we recover the static yz kink energy as $E^o_{yz} \simeq 2\sqrt{\alpha}(1 - \beta^2/16)$, also slightly smaller than the sG result, equation (5-40).

Eliminating s from equations (6-42) obtains the dispersion relation for small velocity:

$$E_{yz}(v) = E^o_{yz} + \frac{1}{2}m^* v^2 \tag{6-45}$$

where the zero velocity rest energy is

$$E^o_{yz} = 2\sqrt{\alpha} r_N^2 - \frac{1}{2}m^* v_0^2 \quad , \tag{6-46}$$

and the effective mass m^* is

$$m^* = [\sqrt{\alpha}\ r_N^2(\frac{2}{\alpha} - \frac{5}{6r_N^2})]^{-1} \simeq \frac{\sqrt{\alpha}}{2r_N^2} \quad . \tag{6-47}$$

This effective mass is consistent with the sG result. Also there is no strange behavior here as for xy kinks; the mass is positive unless $\alpha > \frac{12}{5}r_N^2$, which is too large to be physically possible for real materials. We have shown that these two limiting cases of the full three-parameter Ansatz partially reproduce the sG results (below the critical field) with

slight modifications to the static kink energies. These energy shifts are probably due to using xyz components instead of spherical coordinates. While the yz limit Ansatz is completely consistent with sG theory, the xy limit Ansatz gives indication of an instability which manifests itself through a negative effective mass above the critical field. Next, we present numerical results for E(v) obtained from the full Ansatz, and compare them with dispersion relations obtained from numerical integration of the discrete equations of motion.

6.7 Numerical Results: The Three-Parameter Ansatz vs. Numerical Dynamics

We now present numerical results (see also Wysin et al. 1985) from the three-parameter Ansatz for $\alpha = 0.4$, as appropriate for TMMC (Regnault et al. 1982), and for a series of fields $0.08 < \beta < 0.5$. The parameter θ_A is allowed to vary from zero to π. Here $\beta_c = 0.4$.

The dispersion relation E(v), and $\Delta(\theta_A)$, obtained from the Ansatz, are shown in Figures 6.4 - 6.10. Only those solutions which give $|\Delta| < 0.2$ (an arbitrary cutoff) have been kept. The solid and dashed curves correspond to v_+ and v_- respectively. From the curves of Δ vs. θ_A, and keeping in mind the results of the previous section, it is seen that there are two distinct regions, corresponding to yz-like kinks (the approximately linear portions of $\Delta(\theta_A)$, near $\theta_A = \frac{1}{2}\pi$) or xy-like kinks (the parabolic segments of $\Delta(\theta_A)$, generally at $\theta_A \neq \frac{1}{2}\pi$). For $\beta \neq \beta_c$, there is a small transition region connecting the two. The xy and yz branches are seen to be continuously connected. Also note that the curvature of E_{xy} changes sign at the critical field as in the two parameter Ansatz.

Figure 6.4 Kink energy (in units of JS^2) vs. velocity v (where c = 2) and $\Delta = \theta_B - \theta_A$ vs. θ_A for $\alpha = 0.04$, $\beta = 0.08$. The solid and dashed curves have been obtained from the two solutions given by the Ansatz. The data points are results of the numerical integration of the discrete equations of motion, time averaging initial kink profiles derived from the Ansatz. These comments also apply to Figures 6.5 - 6.10, where the same curves are shown for large fields.

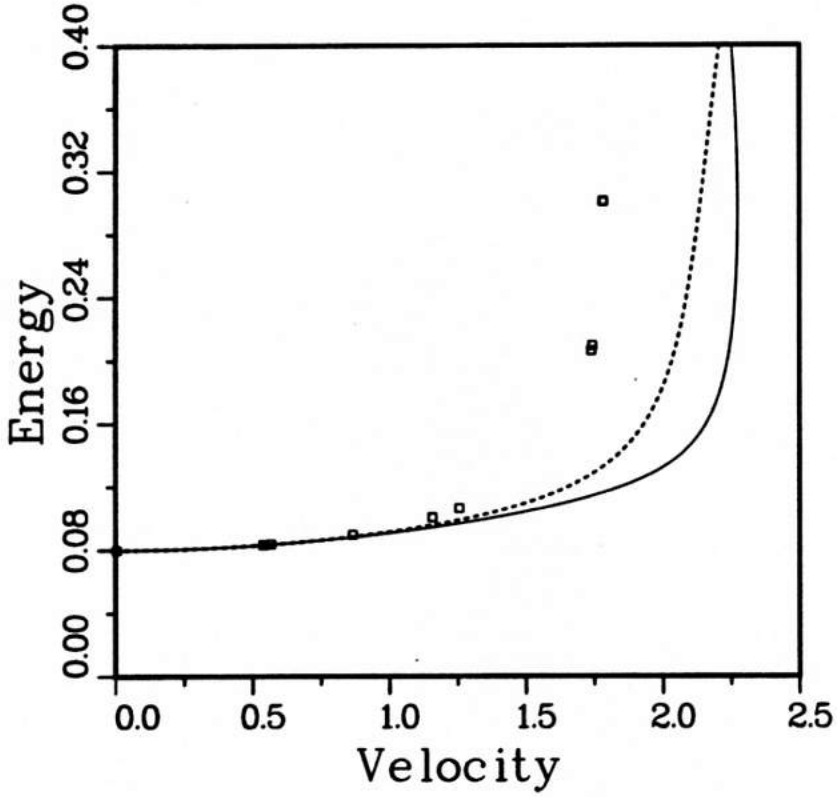
Energy
0.00
0.08
0.16
0.24
0.32
0.40
0.0
0.5
1.0
1.5
2.0
2.5
Velocity

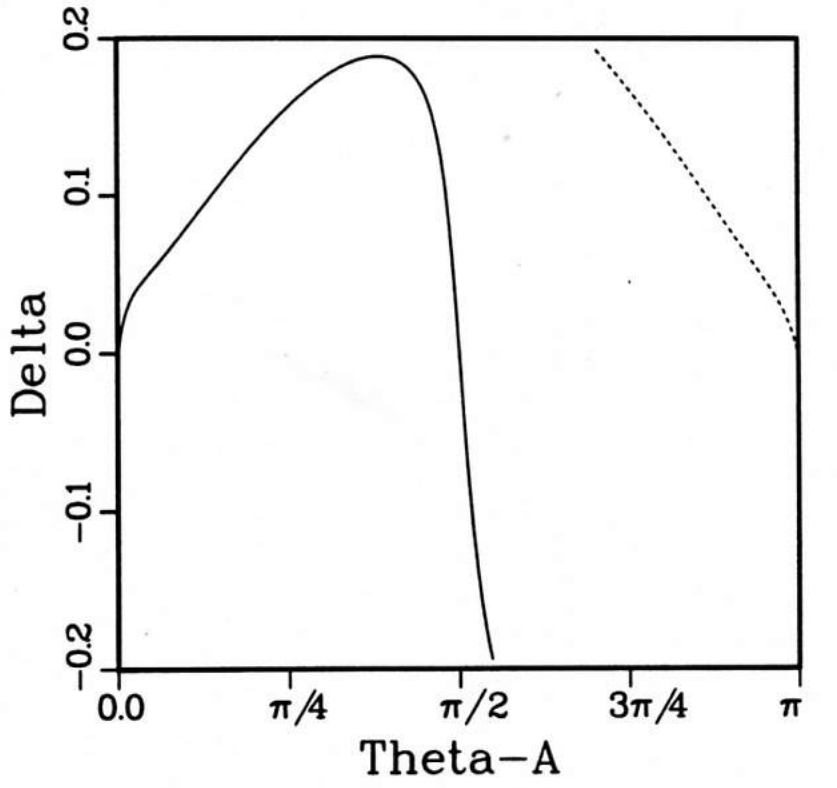
Delta
0.2
0.1
0.0
−0.1
−0.2
0.0
π/4
π/2
3π/4
π
Theta−A

Figure 6.5 Kink energy vs. velocity and Δ vx. θ_A for $\alpha = 0.04$, $\beta = 0.20$. See the Figure 6.4 caption for an explanation.

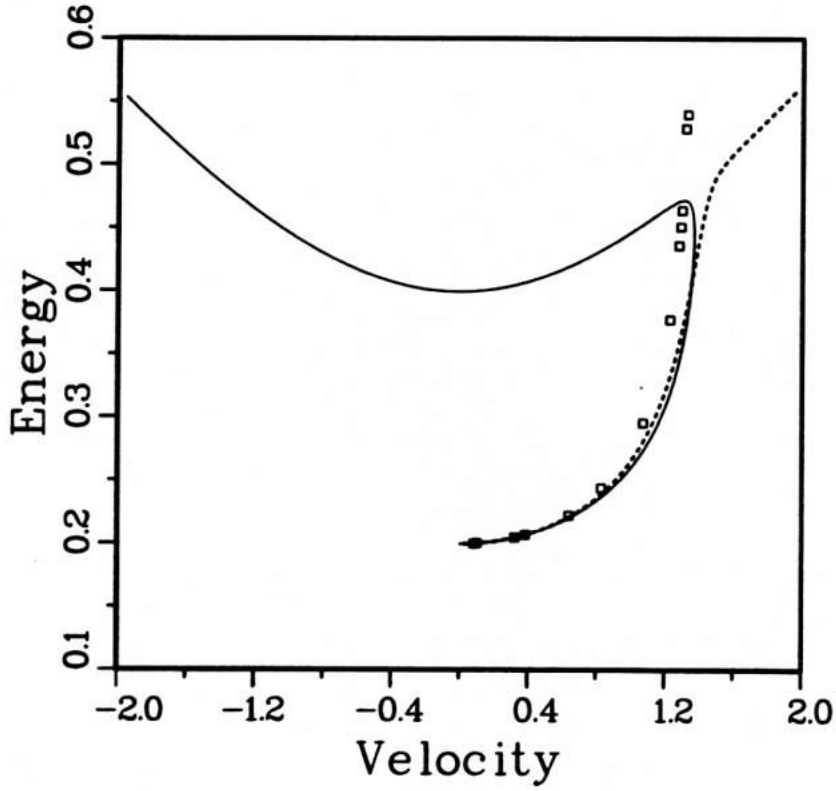
Energy
0.6
0.5
0.4
0.3
0.2
0.1
−2.0
−1.2
−0.4
0.4
1.2
2.0
Velocity

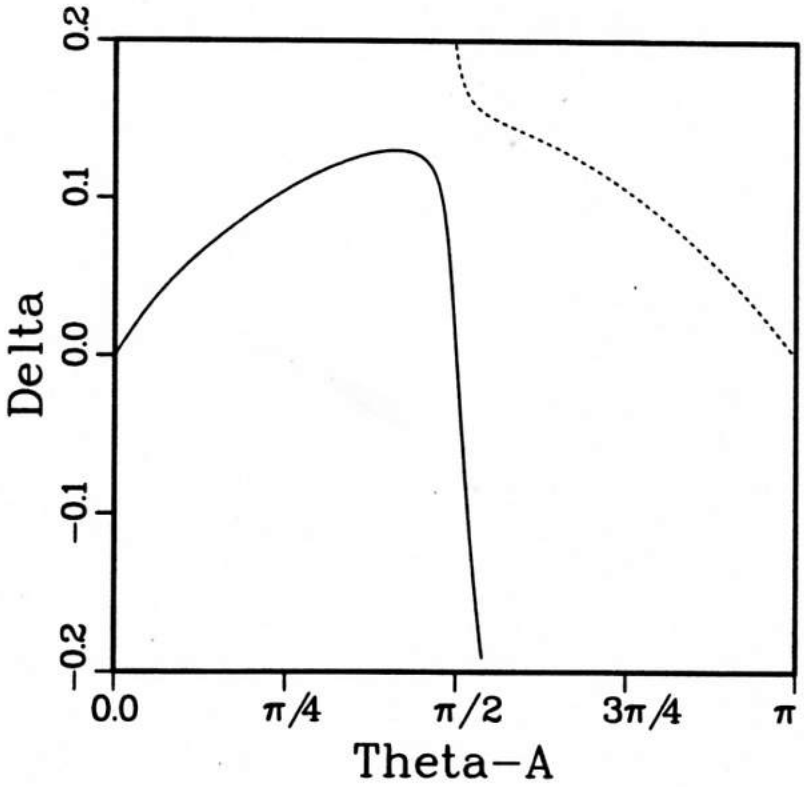
Delta
0.2
0.1
0.0
−0.1
−0.2
0.0
π/4
π/2
3π/4
π
Theta−A

Figure 6.6 Kink energy vs. velocity and Δ vs. θ_A for $\alpha = 0.04$, $\beta = 0.30$. See the Figure 6.4 caption for an explanation. The yz branch kinks are stable above a minimum velocity of $v \tilde{>} 0.65$. Here and in Figure 6.7 = 6.10 it becomes apparent that only the dashed curves given by the Ansatz always correspond to stable kinks.

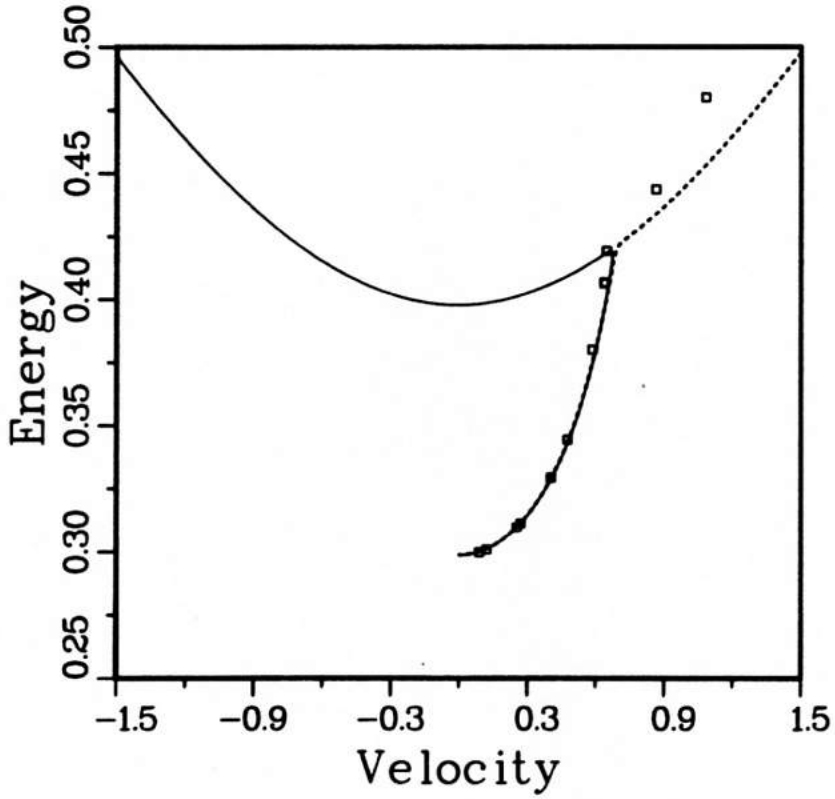
Energy
0.50
0.45
0.40
0.35
0.30
0.25
−1.5
−0.9
−0.3
0.3
0.9
1.5
Velocity

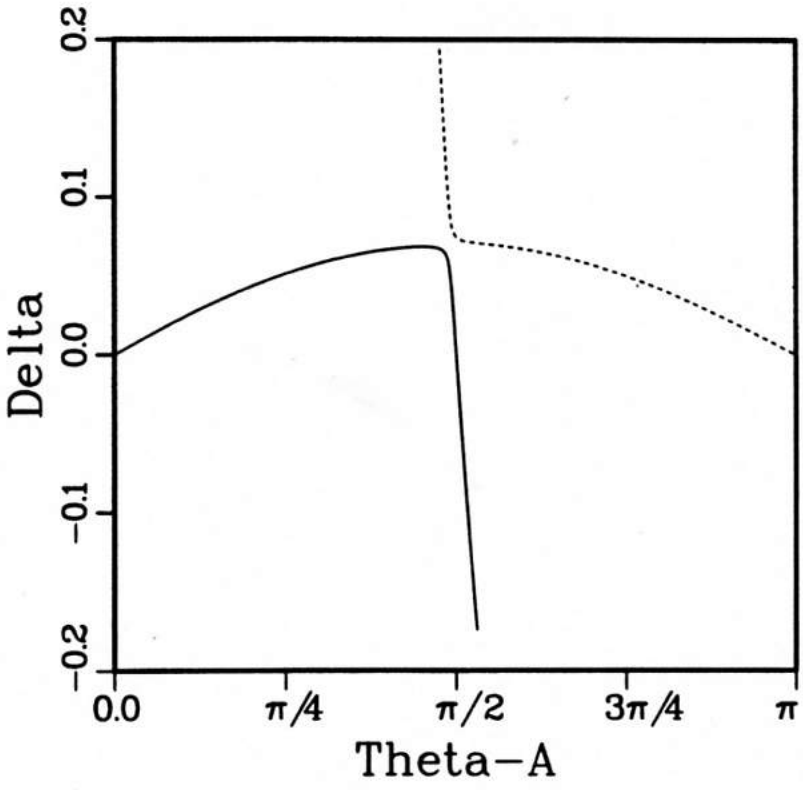
Delta
0.2
0.1
0.0
−0.1
−0.2
0.0
π/4
π/2
3π/4
π
Theta−A

Figure 6.7 Kink energy vs. velocity and Δ vs. θ_A for $\alpha = 0.04$, $\beta = 0.37$. Se the Figure 6.4 caption for an explanation. yz kinks are stable above a minimum velocity of $v \simeq 0.16$.

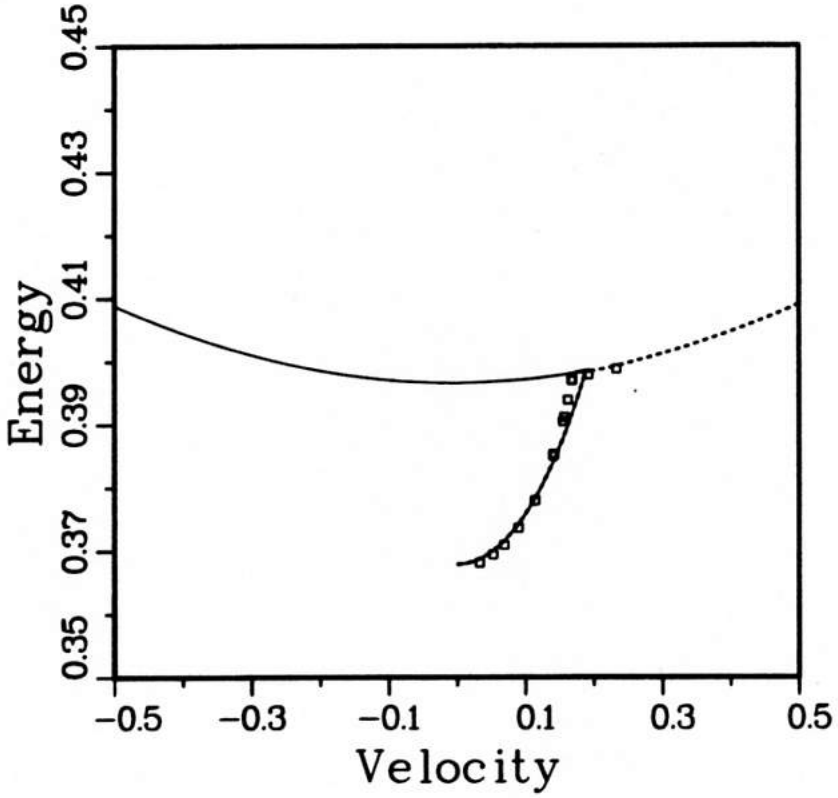
Energy
0.45
0.43
0.41
0.39
0.37
0.35
−0.5
−0.3
−0.1
0.1
0.3
0.5
Velocity

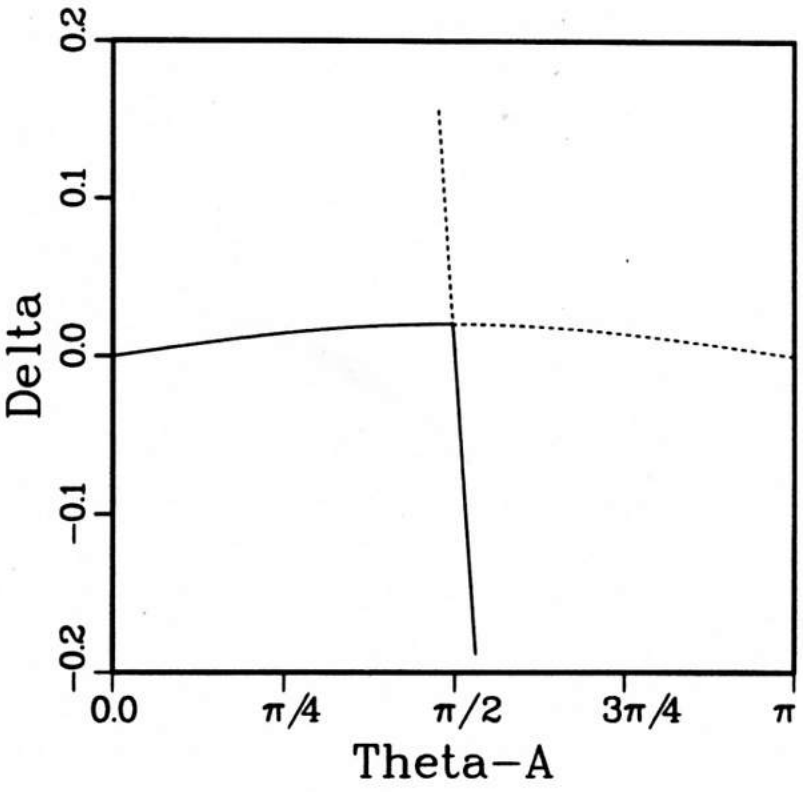
Delta
0.2
0.1
0.0
−0.1
−0.2
0.0
π/4
π/2
3π/4
π
Theta−A

Figure 6.8 Kink energy vs. velocity and Δ vs. θ_A for $\alpha = 0.04$, $\beta = 0.40$, the critical field. See the Figure 6.4 caption for an explanation. The xy branch of E(v) has degenerated to nearly a point. The yz branch is stable only for positive velocities.

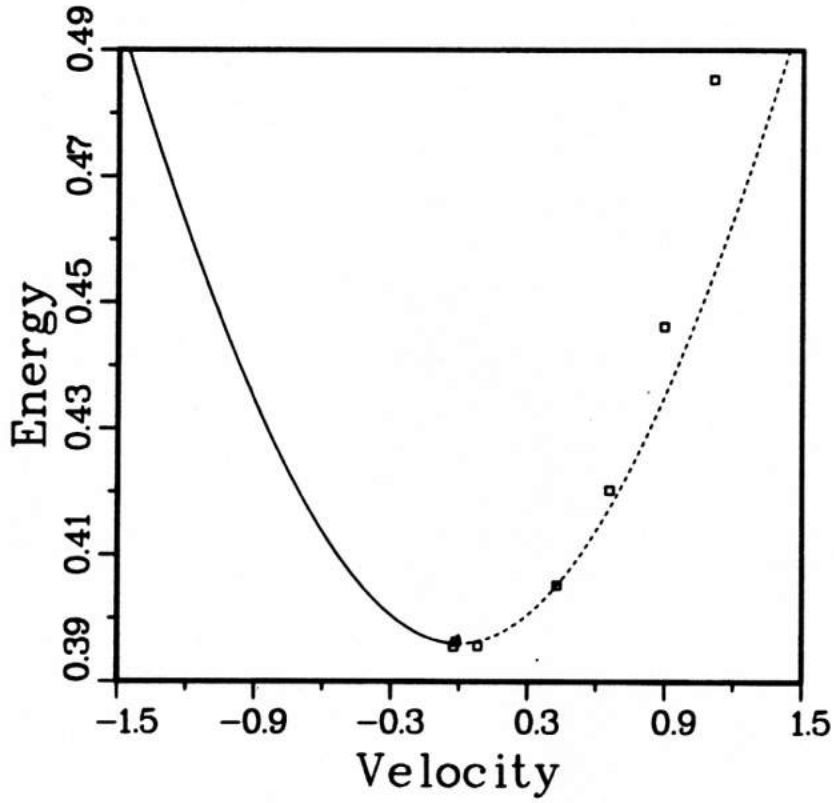
Energy
0.49
0.47
0.45
0.43
0.41
0.39
−1.5
−0.9
−0.3
0.3
0.9
1.5
Velocity

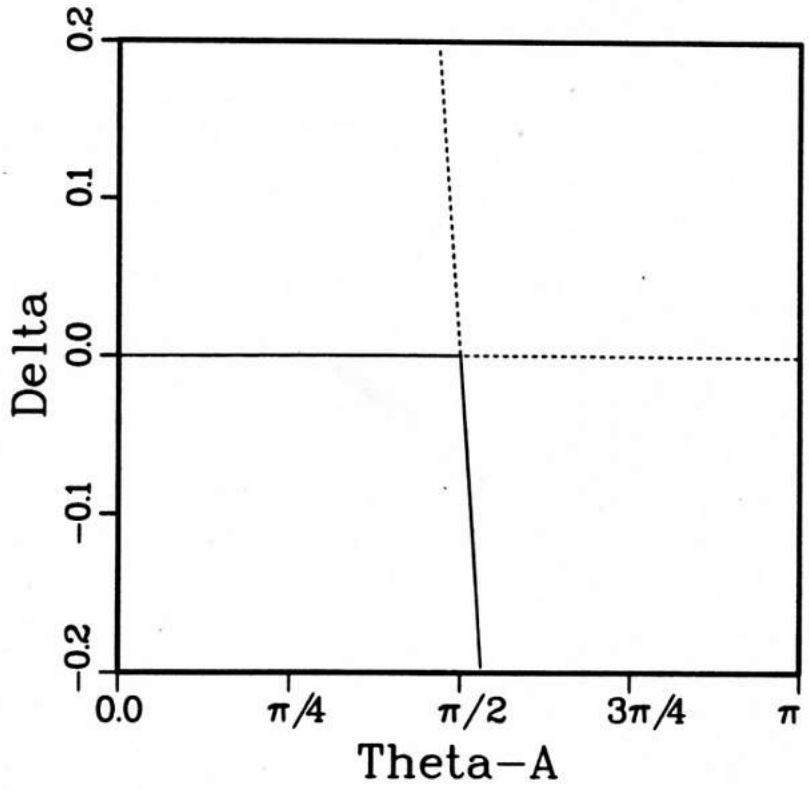
Delta
0.2
0.1
0.0
−0.1
−0.2
0.0
π/4
π/2
3π/4
π
Theta−A

Figure 6.9 Kink energy vs. velocity and Δ vs. θ_A for $\alpha = 0.04$, $\beta = 0.43$. See the Figure 6.4 caption for an explanation. The xy branch kinks now have negative mass. yz branch kink are stable for positive and negative velocities here, down to $v \gtrsim -0.20$.

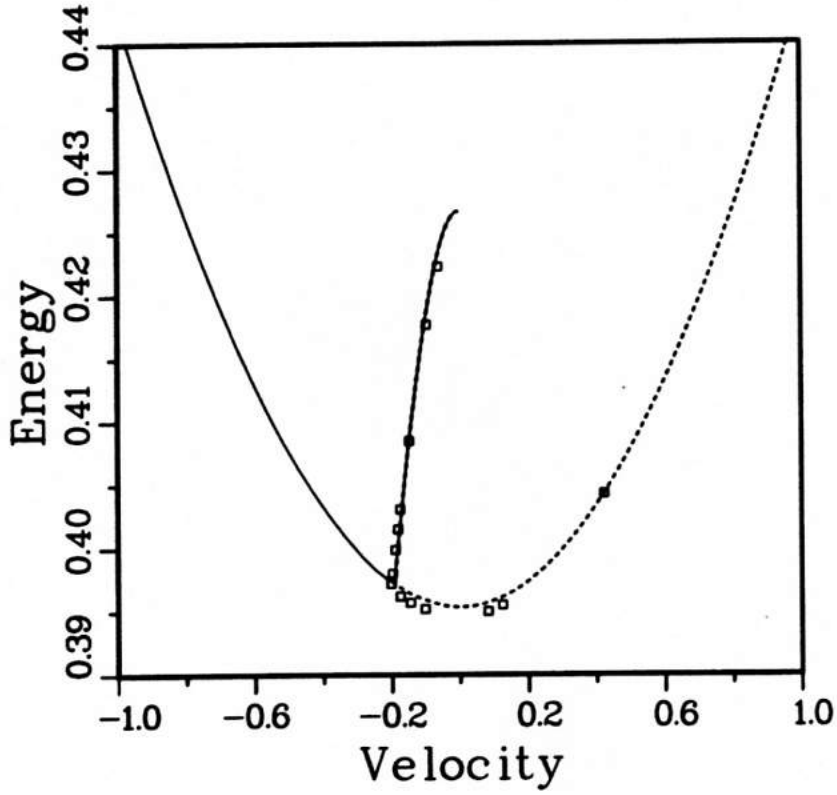
Energy
0.44
0.43
0.42
0.41
0.40
0.39
−1.0
−0.6
−0.2
0.2
0.6
1.0
Velocity

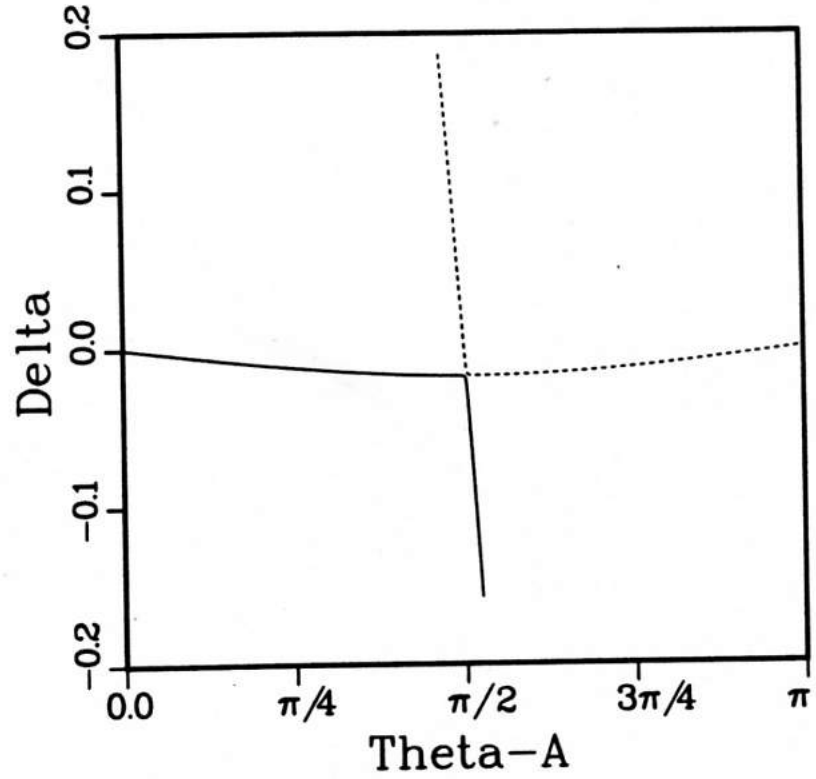
Delta
0.2
0.1
0.0
−0.1
−0.2
0.0
π/4
π/2
3π/4
π
Theta−A

Figure 6.10 Kink energy vs. velocity and Δ vs. θ_A for $\alpha = 0.04$, $\beta = 0.50$. See the Figure 6.4 caption for an explanation. The yz branch is now stable down to $v \simeq -0.55$.

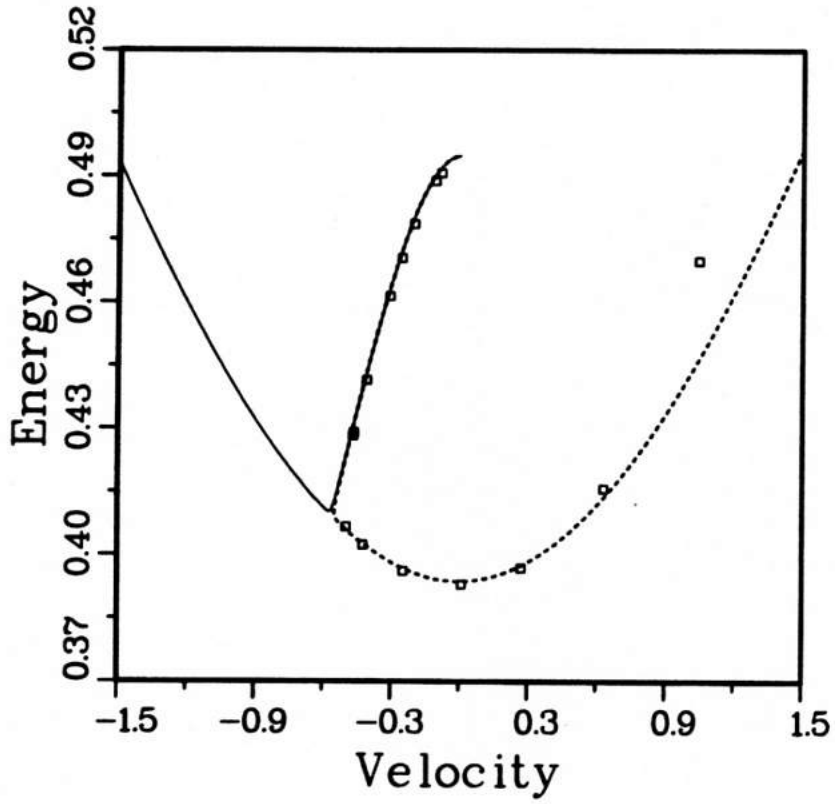
Energy
0.52
0.49
0.46
0.43
0.40
0.37
−1.5
−0.9
−0.3
0.3
0.9
1.5
Velocity

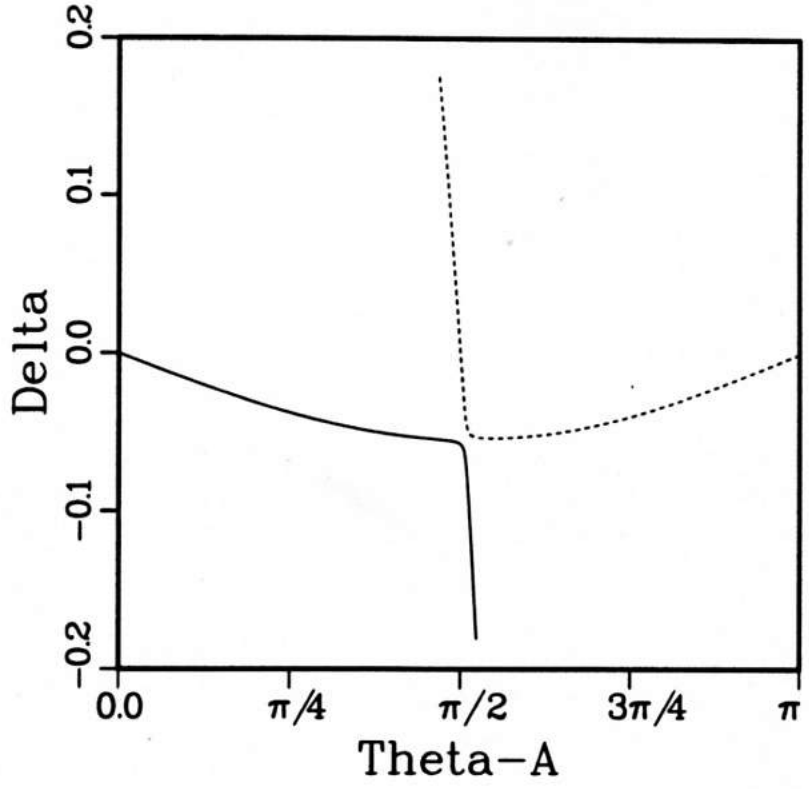
Delta
0.2
0.1
0.0
−0.1
−0.2
0.0
π/4
π/2
3π/4
π
Theta−A

The stability of profiles given by this Ansatz has been determined through numerical integration of the equations of motion on a discrete lattice. The data points in Figures 6.4 - 6.10 were obtained in this way, starting from initial profiles corresponding to both v_+ and v_-. Initial profiles with θ_A over the entire range from zero to π which gave $|\Delta| < 0.2$ were used. Generally, there was relaxation from the initial profile accompanied by spin waves, since the profile was not an exact traveling wave solution to the equations of motion. To remove spin waves, the kink was time-averaged in its own (moving) reference frame, in manner similar to that for the ferromagnet (section 2.6). The difference here, however, is that each sublattice must be averaged separately from the other. An initial profile was time averaged twice for ~ 200 times units before taking data for E(v). Such time averaging usually produces smoother traveling waves, except in cases where discreteness effects are severe (at high velocity) or an instability is nearby in parameter space. The center of the kink is taken to be the point at which $S^y = 0$, interpolated between the lattice points. This definition works equally well for xy and yz kinks. Then the average kink velocity is taken as the average velocity of this center point.

We have used lattices ranging from 101 to 301 spins, depending on the kink width.[1] An odd number of spins is necessary to simulate a system with one kink satisfying periodic boundary conditions. For $\alpha = 0.04$, and $\beta = 0.2$ to 0.6, typical <u>full</u> widths for zero velocity kinks were 10 lattice units for yz kinks and 8-40 lattice units for xy kinks. The equations of motion, written in terms of xyz spin components (equation (2-3) with $J < 0$), were integrated using a fourth order predictor corrector method (Appendix A), with a fixed time step of 0.04. There is a

---

[1] Recall $w_{xy} = 2/\gamma\beta$, $w_{yz} = 1/\gamma\alpha^{1/2}$ in the sG limit.

slight advantage in using xyz components over using spherical polar coordinates, since there are no trigonometric function evaluations, even though there are three equations of motion per spin instead of two. Energy and spin length were both conserved to better than 1 part in 10^5 for the length of these simulations, which were typically 200 to 500 time units (that is, 5000 to 12,500 time steps). This offers a partial check of the numerical accuracy.

Cases where the kink was unstable were obvious. For instance, an unstable yz kink deforms to a lower energy xy kink, accompanied by spin waves. Starting from an Ansatz profile, however, no cases were found where an xy kink decayed into a lower energy yz kink. As a result of these simulations, it was found that only the Ansatz profile corresponding to v_- is always stable. The profile corresponding to v_+ can give an unstable branch. For $\beta < \beta_c$, the static yz kink instability was confirmed. Also for $\beta < \beta_c$, these simulations showed that there is a velocity above which yz kinks <u>are stable</u>, further confirming the linear stability analysis given in Chapter 5. For $\beta = 0.3$, 0.37, 0.43 and 0.5, equation (5-47) gives yz stability limits[1] $v = -0.74$, -0.20, 0.18 and 0.57 respectively. These numbers are consistent with Figures 6.6 through 6.10 if the signs of all velocities are reversed. Note also that this Ansatz shows the xy branches terminating at some velocity less than c, where they meet the yz branch, at <u>its</u> stability limit. For $\beta = \beta_c$, there is a degenerate xy branch (a point).

These numerical simulations were originally performed starting from sG xy or yz initial conditions (as in Chapter 5), using the same time averaging technique. The same dispersion relations were obtained. Also,

---

[1] The "<" sign in (5-47) is somewhat irrelevant. If $\beta^2-4\alpha > 0$, then the origin $v = 0$ is included in the stable regime. If $\beta^2-4\alpha < 0$, then the origin is excluded.

the finite extent of the xy branches was demonstrated. For instance, for $\beta = 0.3$, the Ansatz shows the xy branch terminating into the yz branch near a velocity $v \lesssim 0.7$. If we start with a sG xy kink with $v_{in} > 0.7$, it will "decay" (through the time averaging, which does not conserve energy) to a lower energy yz kink, or a lower velocity xy kink (with $v_{out} < 0.7$!), depending on v_{in}. Similarly the finite extent of the stable yz branches was demonstrated (before the linear stability analysis was available), especially for $\beta < \beta_c$. The yz kinks were found to be stable only if the velocity was greater than the velocity at which the xy branch terminates into the yz branch.

The dispersion relation obtained from numerical dynamics does not agree exactly with that given by the Ansatz calculation, especially for yz kinks, probably due to discreteness effects (for high velocity kinks, width are less than 5 lattice units), along with the small parameter approximations made to evaluate the Lagrangian ($\sqrt{\alpha}$, β, $\Delta \ll 1$). For a kink of given energy, the actual velocity is less than that predicted by the Ansatz or sG theory. This effect is most pronounced for $v/c > 0.5$. Also, we note that kink energies may be slightly overestimated by the numerical integration, since the time averaging technique cannot always completely eliminate spin waves from the system.

6.8 Discussion: Antiferromagnetic xy and yz Kink Behavior

These antiferromagnetic kinks can be compared to the ferromagnetic kinks. In the ferromagnet, recall that the critical field is $\beta_c^{ferro} = \frac{1}{3}\alpha$, while for the antiferromagnet, $\beta_c^{anti} = 2\alpha^{1/2}$. For the antiferromagnet, and $\beta < \beta_c^{anti}$, the xy branch merges into the yz branch at some maximum velocity less than c. In the ferromagnet, for $\beta < \beta_c^{ferro}$, there is also a maximum kink velocity less than c, but there is no sudden change in the

kink profile as one moves along the dispersion through the maximum velocity point. These is only a continuously increasing deviation from the sG profile. However, the xy branch seems to be analogous to the ferromagnetic kinks, in the sense that it becomes a backwards branch for $\beta > \beta_c^{anti}$.

Comparison can be made between this antiferromagnet Ansatz and the Liebmann et al. (1983) ferromagnet Ansatz. In the Liebmann et al. Ansatz, as the variational parameter $\frac{1}{2}\theta_m$ (approximately equivalent to θ_A here) increases from zero to $\frac{1}{2}\pi$, the kink geometry ranges from planar to a small amplitude wave packet, or pulse. The kink branch resulting from their Ansatz therefore terminates at zero energy and velocity, i.e., no kink. In the antiferro-Ansatz here, there is no analogous topological decay of the kink as θ_A is varied from zero to π; the spin profile is always a large amplitude deviation from the ground state configuration, as a result of the boundary conditions. It seems that the boundary conditions strongly affect the dynamics.

We have shown that this Ansatz gives good results by numerical integration of the discrete equations of motion. This was also necessary to test the xy kink stability. A major conclusion drawn from this Ansatz calculation is that the xy and yz kink branches can be considered continuously connected. This is a consequence of the very similar geometries of the xy and yz branches near the point where they merge (see $\Delta(\theta_A)$, in Figures 6.4 - 6.10). Near this merging point, the xy and yz branches have nearly the same θ_A and Δ. Note also that the name "xy kink" is a misnomer; where the "xy" branch merges into the yz branch, θ_A can be very close to $\frac{1}{2}\pi$, and the kink is clearly not a rotation in the xy plane!

The xy kink stability was verified both above and below the critical field, for $\alpha = 0.04$ and $0.08 < \beta < 0.6$. Even for $\beta > \beta_c$, they showed no tendency to decay to lower energy yz kinks, as might be anticipated. Whether they can be viewed as slightly perturbed sG kinks is doubtful, especially for $\beta > \beta_c$. For small velocities $v/c \ll 1$, the two-parameter xy Ansatz reproduced the dispersion and mass as already found by Flüggen and Mikeska (1983), with slight modifications. For $\beta < \beta_c$, the mass is positive and the kinks are close to sG kinks, but move at speeds less than that predicted by sG theory for a given energy. The mass is greater than the sG mass. At the critical field, the mass diverges, and there is a continuum of xy kinks with a range of θ_A, all with the same energy ($= \beta(1 - \beta^2/12)^{1/2}$) and the same velocity ($= 0$). Magyari and Thomas (1983) have referred to this effect in the corresponding ferromagnet as a "soft velocity change". At the critical field, infinitesimal perturbation of a kink (for instance, by varying θ_A) leads to one with the same velocity (and in this case the same energy; the branch has degenerated to a point). Above the critical field, the mass is negative, and there is strong deviation from sG behavior. The situations is the same as in the ferromagnet above the critical field, where the kinks are dynamically stable but move in a direction opposite to that predicted by sG theory (Wysin et al. 1982). It is concluded that xy kinks are not adequately described by sG theory, and that there is no structural (dynamic) instability induced at the critical field, similar to the ferromagnet.

For small velocities $v/c \ll 1$, the two-parameter yz Ansatz reproduces the velocity dependence of the energy as given by sG theory. In general, we find that sG theory adequately describes the yz branch. The stability for yz kinks was checked numerically. For static kinks, the condition for stability $\beta > \beta_c$, as predicted by linear stability analysis, was verified.

Dynamic yz kinks were found to be stable only at velocities greater than the velocity where the xy branch merges into the yz branch. Another way to state this is to say that dynamic yz kinks require a minimum applied field to be stable, where this minimum field decreases with increasing velocity. For $\beta < \beta_c$, a certain amount of canting of the sublattice planes toward the field is necessary to insure stability. For $\beta > \beta_c$, a certain amount of canting of these planes away from the field is allowed before instability results. yz kink stability is determined by both the applied field and the velocity, that is, there is a stability field (a maximum necessary for stability) which depends on the velocity.

All of these results are consistent with experimental data available on TMMC, in particular evidence from neutron scattering experiments (Boucher et al. 1984) for a crossover from xy to yz kinks at high field. We find stable xy kinks exist both above and below the critical field, as well as stable yz kinks existing both above and below the critical field. Therefore, generally both types of kinks carry thermodynamic weight at an arbitrary field, but this is especially important near the critical field. A careful analysis should be able to make predictions for experimentally measurable thermodynamic quantities (for $\beta \sim \beta_c$), especially since the general kink stability has been determined. Further information concerning kink stability during collisions would also be useful, but is not presently available.

Up to now we have considered only classical 1-D magnets, and their nonlinear excitations. In Part II, we turn to the statistical mechanics of quantum 1-D ferromagnets, described by the quantum version of the Hamiltonian under consideration so far. The elementary nonlinear excitations in themselves will not be studied, since quantum Monte Carlo techniques will be employed, which give only statistical thermodynamic

information. Data obtained numerically will be compared with experiments available for the easy plane ferromagnets CHAB (spin $S = \frac{1}{2}$) and $CsNiF_3$ (spin $S = 1$).